JOURNAL OF COMPUTATIONAL PHYSICS 24, 398–415 (1977)

The Vector and Scalar Potential Method for the Numerical Solution of Two- and Three-Dimensional Navier–Stokes Equations

Y. A. S. AREGBESOLA

Department of Mathematics, University of Ife, Ile-Ife, Nigeria

AND

D. M. BURLEY

Department of Applied Mathematics and Computing Science, The University, Sheffield S10 2TN, England

Received July 21, 1976; revised December 6, 1976

A method is presented for the numerical finite-difference solution of the equations of motion for laminar, incompressible steady-state flow in both two and three dimensions. The complete Navier–Stokes equations are transformed and expressed in terms of vorticity, scalar, and vector potentials. The transformed equations are solved iteratively. The method is evaluated by solving the Navier–Stokes equations in a plane groove region. Numerical solutions of three-dimensional flows in a square duct and in a rectangular cavity formed in one wall of a square duct are presented. The results obtained are compared with the experimental results and other calculations.

1. INTRODUCTION

A suitable method for the numerical solution of steady-state equations for laminar incompressible flows both in two and three dimensions consists of a transformation of the complete Navier–Stokes equations in terms of a vector vorticity, a vector potential, and a scalar potential. The approach is based on work of such authors as Aziz and Hellums [1], Mallinson and de Vahl Davis [2], Holst and Aziz [3] to mention a few, for the numerical solution of the three-dimensional equations of motion for laminar natural convection in a confined region.

The main difficulty encountered by earlier users of this approach was in the setting of the boundary conditions on the vector potential in the most convenient form. This difficulty is in direct contrast to the two-dimensional approach of the stream function-vorticity method, where finding restrictions on the stream function on the boundary is relatively simple. The specification of boundary conditions on both scalar and vector potentials has been fully discussed by Hirasaki and Hellums [4, 5].

This approach has been used to solve laminar natural convection flows in a confined region, but in this paper it is used to solve more difficult problems in regions with inlet and outlet flows.

ISSN 0021-9991

2. The Equations of Motion

The dimensionless equations describing a viscous incompressible laminar steady-state flow in vector form are

$$\nabla \cdot \mathbf{V} = 0, \tag{2.1}$$

$$(\mathbf{V} \cdot \nabla)\mathbf{V} = -\nabla P + (1/\mathrm{Re})\,\nabla^2 \mathbf{V}, \tag{2.2}$$

where in Cartesian coordinates, $\mathbf{V} = (u, v, w)$ is the velocity, P is the pressure, and $\mathrm{Re} = L\rho_0 U_0/\mu_0$ is the Reynolds number, L, ρ_0, U_0, and μ_0 are representative length, density, velocity, and viscosity, respectively. Taking the curl of Eq. (2.2) gives

$$(\mathbf{V} \cdot \nabla)\boldsymbol{\xi} - (\boldsymbol{\xi} \cdot \nabla)\mathbf{V} = \nabla^2 \boldsymbol{\xi}/\mathrm{Re}, \tag{2.3}$$

where $\boldsymbol{\xi} = \nabla \wedge \mathbf{V}$ is the vorticity. To satisfy Eq. (2.1) identically the scalar potential, Φ, and the vector potential, $\mathbf{A}$, are introduced through the equation

$$\mathbf{V} = -\nabla\Phi + \nabla \wedge \mathbf{A}. \tag{2.4}$$

A unique vector potential $\mathbf{A}$, within the gradient of an arbitrary harmonic function, exists such that

$$\nabla \cdot \mathbf{A} = 0 \tag{2.5}$$

as already demonstrated in [5]. Taking the divergence of Eq. (2.4) gives

$$\nabla^2\Phi = -\nabla \cdot \mathbf{V} = 0 \tag{2.6}$$

and the condition

$$\partial\Phi/\partial n = -\mathbf{n} \cdot \mathbf{V}$$

is chosen on the boundaries, where $\mathbf{n}$ is a unit vector normal to the boundary at each point. Equation (2.6) has a solution if and only if

$$\int_R \nabla^2\Phi \, dV = \int_R \nabla \cdot \nabla\Phi \, dV = \int_S \nabla\Phi \cdot d\mathbf{S} = \int_S (\partial\Phi/\partial n)\, dS = 0, \tag{2.7}$$

where S denotes the surface enclosing the volume R. In this case a solution is obtained to within an arbitrary constant but since the gradients of the scalar potential only are required, the arbitrary constant is irrelevant. It should be noted that for problems with no inflow and outflow, $\mathbf{V} = 0$ on all the boundaries so that (2.6) has the trivial solution $\Phi \equiv 0$ and hence the scalar potential is not required for such problems.

By taking the curl of Eq. (2.4) and applying (2.5) a differential equation for the vector potential is derived as

$$\nabla^2 \mathbf{A} = -\boldsymbol{\xi}. \tag{2.8}$$

Boundary Conditions

The normal velocity components are assumed to be known and these values are used in the normal derivatives of the scalar potential on the boundary.

The boundary conditions on the vector potential **A** are chosen such that the tangential components of **A** are equal to zero and the condition on the normal component is then determined by the solenoidal condition, $\nabla \cdot \mathbf{A} = 0$. For a flat boundary the conditions become

$$\partial A_n/\partial n = 0, \qquad \mathbf{A}_t = 0.$$

By this choice the normal velocity to the surface is determined by $-\partial\Phi/\partial n$ and is not altered by the vector potential as can be seen from (2.4). In addition, it has been shown in [4, 5] that with the above boundary conditions the vector potential is unique.

Having dealt with normal velocities on the boundaries, the tangential velocities, which are usually zero on the boundaries, are used in the setting up of the boundary conditions on the vorticity. They are incorporated appropriately in the components of the vorticity, $\xi = \nabla \wedge \mathbf{V}$, where **V** is calculated from ϕ and **A** by (2.4).

3. Finite-Difference Approximations

An interlaced uniform mesh is used. A diagram to illustrate the coordinate systems for each variable is shown in Fig. 1. The choice of the interlaced mesh system was

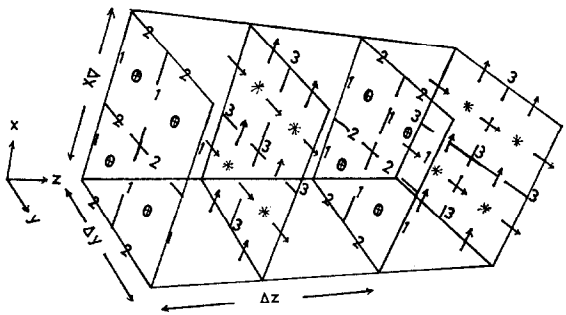

FIG. 1. *-points are at the center of basic fluid elements and these are the scalar potential points. 1-points are for the A_1 and ξ_1 ; 2-points are for the A_2 and ξ_2 ; 3-points are for the A_3 and ξ_3 . ⊕-points are for the axial velocity, w; → points are for the transverse velocity v; and ↑-points are for the vertical velocity u.

found necessary mainly to cope more easily with the derivative type of boundary conditions on the variables involved. The system enables the walls to lie midway between the last or first two mesh points in each direction so that the central finite-difference scheme for the gradient of the variable can be applied. In this way the truncation error, introduced as a result of the finite-difference approximation of the

derivative, $\partial\Phi/\partial n$, on the boundary has the leading term reduced from $\frac{1}{6}h^2\partial^3\Phi/\partial x^3$ to $(1/24)\,h^2\partial^3\Phi/\partial x^3$ with the interlacing mesh system, where h is the mesh spacing.

The finite-difference approximations for the x-component of the vector vorticity equations will only be discussed. The other components are similar. Mesh point variables are denoted by (I, J, K) and the notation is used in which, for instance, $\Phi(I-1)$ represents $\Phi(I-1, J, K)$. The x-component of the vorticity equation from (2.3) is

$$\left(\frac{\partial^2\xi_1}{\partial x^2}+\frac{\partial^2\xi_1}{\partial y^2}+\frac{\partial^2\xi_1}{\partial z^2}\right)\Big/\mathrm{Re} = u\frac{\partial\xi_1}{\partial x}+v\frac{\partial\xi_1}{\partial y}+w\frac{\partial\xi_1}{\partial z} - \xi_1\frac{\partial u}{\partial x}-\xi_2\frac{\partial u}{\partial y}-\xi_3\frac{\partial u}{\partial z}. \tag{3.1}$$

To approximate the convection terms, namely

$$u(\partial\xi_1/\partial x)+v(\partial\xi_1/\partial y)+w(\partial\xi_1/\partial z), \tag{3.2}$$

at the ξ_1 points, the partial derivatives are replaced by their finite-difference equivalents half a mesh length upstream of ξ_1 points. Such an "upwind difference" technique has been used extensively since its introduction by Courant *et al.* [6], also see, for example, Hellums and Churchill [7] and Gosman *et al.* [8]. The method is required to stabilize the numerical iterations for higher Re (say $\geqslant 50$). The resulting difference equations are diagonally dominant and this helps to promote numerical stability. At lower Re the convection terms are small compared with the diffusion terms so the upwind differencing has little effect at these Re. Thus in the first term of (3.2), with $\Delta x = X_{I+1} - X_I$,

(a) $u^{\mathrm{AV}} > 0$, $\quad \partial\xi_1/\partial x$ is replaced by $(\xi_1 - \xi_1(I-1))/\Delta x$,

(b) $u^{\mathrm{AV}} < 0$, $\quad \partial\xi_1/\partial x$ is replaced by $(\xi_1(I+1) - \xi_1)/\Delta x$,

and the other terms follow similarly. Here the superscript AV indicates the velocity at the ξ_1 points, determined by the average over the immediate neighboring points where u is evaluated explicitly in the interpenetrating mesh. Thus with the labeling used in the program

$$u^{\mathrm{AV}} = (u(J+1, K+1)+u(K+1)+u(J+1)+u(I-1, J+1)+u + u(I-1, J+1, K+1)+u(I-1, K+1)+u(I-1))/8.$$

With the above schemes, the approximation to (3.2) gives

$$\text{Convection terms} = -C_P\xi_{1P}+C_N\xi_{1N}+C_S\xi_{1S}+C_F\xi_{1F} + C_H\xi_{1H}+C_E\xi_{1E}+C_W\xi_{1W}$$

where P, N, S, F, H, E, and W are as displayed in Fig. 2; and

$$C_N = (|\, U^{AV} \,| - U^{AV})/2\Delta x, \qquad C_S = (|\, U^{AV} \,| + U^{AV})/2\Delta x, \quad \text{etc.}$$
$$C_P = C_W + C_E + C_F + C_H + C_N + C_S\,,$$

where all the C's are now nonnegative. The source terms

$$\xi_1(\partial u/\partial x) + \xi_2(\partial u/\partial y) + \xi_3(\partial u/\partial z) \tag{3.3}$$

are represented at the ξ_1 points by average values over immediate neighbors where the values are explicitly evaluated. Thus (3.3) is approximated as

$$\xi_1(\partial u/\partial x)^{AV} + \xi_2^{AV}(\partial u/\partial y)^{AV} + \xi_3^{AV}(\partial u/\partial z)^{AV}$$

where for example

$$(\partial u/\partial x)^{AV} = (u(J+1, K+1) + u(K+1) + u(J+1) + u - u(I-1, J+1, K+1)$$
$$- u(I-1, K+1) - u(I-1, J+1) - u(I-1))/4\Delta x,$$

and

$$\xi_2^{AV} = (\xi_2(J+1) + \xi_2(I-1, J+1) + \xi_2 + \xi_2(I-1))/4,$$

and the other terms similarly. It is possible to leave the ξ_1 term of (3.3) as an unknown in this ξ_1 equation. However the difference equations would not necessarily remain

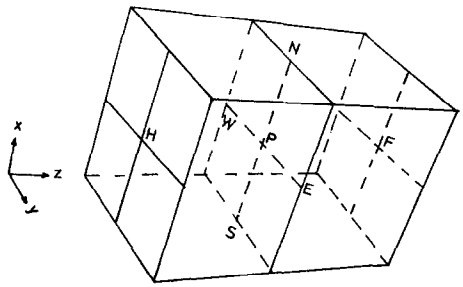

FIG. 2. The nodal points surrounding any point P.

diagonally dominant and it seems reasonable to leave all the source terms together. Thus all the terms in (3.3) were treated as source terms, evaluating them from current values in the iteration cycle. As for the diffusion terms on the L.H.S. of Eq. (3.1) a conventional central difference scheme is used on the Laplacian. After some rearrangement the finite-difference equation for the ξ_1 equation becomes

$$\xi_{1P} = (D_E\xi_{1E} + D_W\xi_{1W} + D_F\xi_{1F} + D_H\xi_{1H} + D_N\xi_{1N} + D_S\xi_{1S} + S_1)/\Sigma D_M$$

where M takes the values of $E, W, F, N,...$, and

$$D_N = C_N + (1/\mathrm{Re}\,\Delta x^2), \qquad D_S = C_S + (1/\mathrm{Re}\,\Delta x^2) \quad \text{etc.}$$

and S_1 is the finite-difference representation of the expression in (3.3). All the D's are now strictly nonnegative from the upwind differencing.

The finite-difference equivalents of the vector potential equations and the scalar potential equation are simple, just being Poisson and Laplace equations, and will not be discussed here. Representations of the boundary conditions for the scalar and vector potentials are straightforward too. Boundary conditions on the vorticity are derived from the definition $\xi = \nabla \wedge \mathbf{V}$. Unlike the stream function-vorticity method, where the vorticity is expressed in terms of the stream function, it is most convenient with the vector potential method to express the vorticity in terms of the velocities.

Consider, for instance, the vorticity

$$\xi_1 = (\partial w/\partial y) - (\partial v/\partial z)$$

on a plane $z = 0$. Since all the components of the velocities are zero, $\partial w/\partial y = 0$ and with the mesh system used, $\xi_1(x, y, 0)$ may be approximated by

$$\xi_1(x, y, 0) = -(9v(x, y, \tfrac{1}{2}h) - v(x, y, \tfrac{3}{2}h))/3h. \tag{3.4}$$

The leading truncation error is of order h^2. This one-sided approximation is necessary because the velocity components outside the boundary are not known. However, when the velocity components on the boundary are known and are required to calculate the vorticity on the boundary, the values of the velocity on the boundary must be

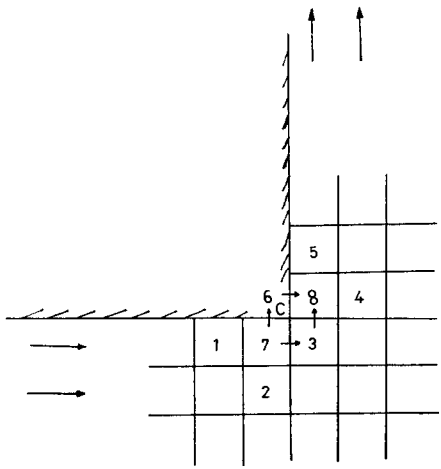

FIG. 3. A reentrant corner at point C.

used. A reentrant corner shown in Fig. 3 is an example of this situation. The arrows show the velocity components to be used in the approximation of the velocity gradient at the illustrated point. For instance care has to be taken in calculating the values of Φ at the points like 7 and 8 shown in the diagram. Two values are required at point 6. One to satisfy the boundary condition between points 6 and 8 and the other to satisfy the boundary condition between points 6 and 7.

4. General Solution Procedure

The numerical solution of Φ equation (2.6) is obtained independently of other equations for the situations considered in this paper. The cycle of iteration for the solution of the remaining equations consists of

(a) calculation of new vorticity boundary conditions from the current velocity values;

(b) computations of new values of the vorticity ξ at the interior points from the appropriate finite-difference equation;

(c) calculation of new vector potential boundary conditions;

(d) computation of new values of the vector potential, **A**;

(e) calculation of new velocity components from the current scalar and vector potentials.

For the components of the vector potential, **A**, and the scalar potential, over-relaxation was used for the iteration and the relaxation parameters used lie between 1.4 and 1.7. The use of underrelaxation was necessary for the solution of the vorticity equations. The underrelaxation parameter decreases with increase in the Reynolds number. It was not possible to obtain a useful mathematical formula for the relationship between Re and this underrelaxation parameter, and it was left to experience to set it at an appropriate value, usually between 0.25 and 0.75.

The accuracy of this method greatly depends on the accurate solution of the Laplace equation since this represents the continuity equation. It was therefore found necessary to let

$$| \Phi^n - \Phi^{n-1} | < 5 \times 10^{-6}$$

where Φ^n denotes a value of Φ in the nth cycle of iteration. In arriving at the conditions given above it was observed that the rate of convergence is very slow, perhaps this is due to the nature of the boundary conditions imposed on the variable Φ.

All the calculations performed in this paper used either the University of Sheffield 1907 ICL computer or, for the bigger problems, the University of Manchester Regional computer, CDC 7600.

5. Application to a Two-Dimensional Flow

The method when applied to standard two-dimensional problems, for example the entrance length between parallel plates, gave results that agree satisfactorily with other methods. It was, therefore, applied to a more complicated geometry to provide a more severe test.

The method is applied to the solution of a flow in a plane groove and the region of integration is as shown in Fig. 4. At the inlet the velocity is assumed constant while a parabolic profile is assumed at the outlet such that

$$w = 1, \qquad u = 0 \qquad \text{for} \quad z = 0, \qquad 0 \leqslant x \leqslant 1 \tag{5.1}$$

and

$$w = 6(x - x^2)\, \Sigma w(0)/\Sigma w(z_3), \qquad u = 0 \text{ for } z = z_3, \quad 0 \leqslant x \leqslant 1, \tag{5.2}$$

where $\Sigma w(0)$ and $\Sigma w(z_3)$ are the sums of the normal velocities at $z = 0$ and $z = z_3$, respectively. The ratio $\Sigma w(0)/\Sigma w(z_3)$ is used to conform with the condition in (2.7). This is necessary since the finite-difference method chosen imposes an integration procedure for the integrals in (2.7) and the ratio corrects small numerical errors in the integration method.

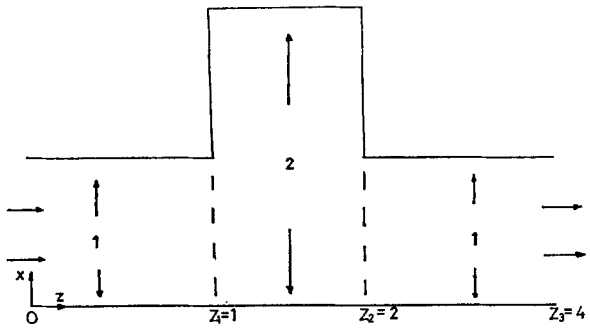

FIG. 4. Schematic drawing of the plane groove geometry with $0z_1 = 1$, $0z_2 = 2$, $0z_3 = 4$.

Some of the data obtained from the plane groove problem with Re = 50 are tabulated in Tables I and II for comparison between the stream function-vorticity method and the vector potential method.

These results show a reasonable agreement, although it should be noted that the problem was solved with different mesh lengths in each approach. With the stream function-vorticity method a 41 × 41 mesh point system was used with $\Delta x = 0.05$ and $\Delta z = 0.1$, while a 21 × 41 mesh point system was used for the vector potential method with $\Delta x = \Delta z = 0.1$. This choice makes some of the axial velocity points coincide in the two systems for comparison purposes. The difference in the mesh lengths may account for the slight differences in the tabulated results, since a decrease in the mesh lengths will improve the accuracy.

TABLE I

Numerical Data for the Axial Velocity, w, in the Solution of a Flow Problem in a Plane Groove, Re = 50[a]

	z											
x	0.00	0.10	0.20	0.30	1.10	1.50	1.90	2.30	2.80	3.40	4.00	
0.25	1.000	1.052	1.119	1.161	1.076	1.018	1.025	1.076	1.118	1.129	1.128	SVM
	1.000	1.048	1.118	1.162	1.090	1.041	1.043	1.083	1.118	1.126	1.121	VPM
0.95	1.000	0.818	0.643	0.530	0.497	0.590	0.501	0.351	0.290	0.283	0.283	SVM
	1.000	0.839	0.651	0.521	0.468	0.571	0.542	0.337	0.287	0.283	0.283	VPM

[a] SVM = results with stream function vorticity method $\Delta x = 0.05$, $\Delta z = 0.1$. VPM = results with vector potential method $\Delta x = \Delta z = 0.1$.

TABLE II

Numerical Data for the Axial Velocity, w, in the Solution of Flow Problem in a Plane Groove, Re = 50[a]

	z	
x	$\frac{1}{2}(z_1 + z_2)$	
0.05	0.258	0.262
0.15	0.697	0.711
0.25	1.018	1.041
0.45	1.306	1.340
0.65	1.252	1.284
0.85	0.873	0.872
1.05	0.349	0.309
1.25	0.0563	0.0253
1.45	−0.0371	−0.0533
1.65	−0.0452	−0.0511
1.85	−0.0266	−0.0279
1.95	−0.0108	−0.0114
	SVM	VPM

[a] SVM and VPM are as in Table I.

A typical computer time for the stream function-vorticity method was about 500 seconds on ICL 1907 (roughly equivalent to 10 seconds on CDC 7600) starting from zero initial values. For the vector potential method a similar time was used once the scalar potential had been calculated. The solution of the Laplace equation for Φ with Neumann conditions round the whole boundary was found to be extremely slow and to take more or less the same computer time as the rest of the iteration cycle. However for the same configuration once Φ is known it can be used for all Re.

6. Three-Dimensional Calculations

One of the difficulties in three-dimensional work is that suitable theoretical and experimental data is only just becoming available to provide a check on the accuracy and applicability of a method. For the standard problem of the entrance region into a square duct there is sufficient data for useful comparisons to be made.

A detailed comparison of some results has already been made with the present method by Roscoe [10]. He develops and describes a primitive variable method of his own and then compares his results with those obtained from the program used in this paper. He studied the development of the flow, at Re $= 1.5$, in a square duct from a step function inlet profile; on one-half of the duct the inlet velocity is 1 and on the other half it is 2. His general conclusion is that there is excellent agreement between the two methods on the flow development along the duct; across the section of the duct the quantitative agreement is good for low-value velocities and moderate for high values of velocity. Typical computer times for this problem are 5 minutes and 11 minutes on a CDC 7600 for Roscoe's and the present program, respectively, starting from initial values of zero for all variables. As with all iterative methods much faster times can be achieved with a good first guess, for instance, the results from the nearest available case.

A major limitation on the work is the storage capacity of computers. A $15 \times 15 \times 15$ mesh tests the limits of a computer, while experience in two dimensions suggests that good quantitative accuracy would require a $30 \times 30 \times 30$ mesh. Such a size is beyond even the largest machines. However the work already performed suggests that comparatively coarse meshes give useful qualitative results and encouragement that meaningful and interesting work can be performed on present day machines in computer times of 5–10 minutes per run.

Associated with three-dimensional calculations is the problem of how to reduce large amounts of computed data into an easily assimilated form. In two dimensions it is easy to draw and interpret stream function contours but in three dimensions the contours of scalar or vector potential are neither easy to draw nor to interpret. It is desirable to present the vector velocity $\mathbf{V} = (u, v, w)$ over the whole three-dimensional mesh. In an attempt to give an impression of the three-dimensional nature of the flows, perspective drawings of the configuration are presented with $\mathbf{V}$ given on particular planes.

7. Flow in a Square Duct

The configuration studied here is the flow in a square duct defined by $0 \leqslant x \leqslant 1$, $0 \leqslant y \leqslant 1$, $0 \leqslant z \leqslant z_1$.

At the inlet $z = 0$, a uniform inlet profile is assumed so that

$$u = v = 0, \qquad w = 1, \qquad \Phi_z = -1,$$
$$A_1 = A_2 = \partial A_3/\partial z = 0, \qquad \xi_1 = -\partial v/\partial z, \qquad \xi_2 = \partial u/\partial z, \qquad \xi_3 = 0.$$

At the outlet $z = z_1$, it is assumed that the flow has reached its fully developed profile, so that

$$u = v = 0, \qquad w = w_1, \qquad \Phi_z = -w_1,$$
$$A_1 = A_2 = \partial A_3/\partial z = 0, \qquad \partial \xi_1/\partial z = \partial \xi_2/\partial z = \xi_3 = 0,$$

and w_1 is given by

$$w_1 = \frac{\pi^2}{4}\left\{\sum_{m,n=1,3,5,\ldots}^{\infty} \frac{\sin m\pi x \sin n\pi y}{mn(m^2+n^2)} \Big/ \sum_{m,n=1,3,5,\ldots}^{\infty} \frac{1}{m^2n^2(m^2+n^2)}\right\}, \tag{7.1}$$

see for instance Han [11].

On the solid boundaries $x = 0, 1$, $y = 0, 1$, the conditions are taken directly from Sections 2 and 3.

The major problem in the computation is the solution of the Laplace equation for the scalar potential Φ. The difficulty is created by the Neumann boundary conditions round the whole of the boundary. The final difference equations for Φ take the form $\mathbf{Ax} = \mathbf{b}$, where the sum of the rows of the matrix $\mathbf{A}$ are zero. Unfortunately the sum of the elements of $\mathbf{b}$ are not identically zero because of small numerical errors in the difference scheme used. The w_1 defined in (7.1) is modified as in (5.2) to ensure that the amount of fluid entering is the same as that leaving. The correction was found to be necessary since significant errors propagated into the solution without it. This problem proved to be more acute in three-dimensional calculations than in two dimensions. Although the convergence was slow, a point SOR method converged to what is effectively the inviscid, irrotational solution to the problem. Viscous and rotational effects were incorporated in the remaining iteration cycle described in Section 4.

Results were obtained for Re = 1, 50, 100. Typically for the case Re = 50 a $13 \times 13 \times 32$ mesh was used with $\Delta x = \Delta y = 1/11$ and $\Delta z = \frac{1}{6}$. Starting with an initial guess obtained by interpolating between the inlet and outlet (where possible) this case, including the scalar potential calculation, took 166 seconds on CDC 7600.

Other theoretical calculations found for this problem use some approximate equations, usually the boundary layer equations, for example Han [11], Briley [12]. These solutions cannot be expected to be accurate near the duct entrance where there is a strong viscous, inviscid core interaction. The major experimental work was

performed by Goldstein and Kreid [13]. Again in experimental work it is difficult to reproduce the sharply singular inlet profiles used in the theoretical calculations so that comparisons very close to the inlet are not particularly reliable.

The major parameter calculated and measured in experiments is the entrance length, defined as the distance down the duct required for the flow to reach 99% of fully developed flow values. For the three cases Re = 1, 50, 100 the values obtained by the present analysis were $z/\mathrm{Re} = 0.742, 0.087, 0.086$, respectively. As with the corresponding two-dimensional problem, a more or less steady value of z/Re is obtained for Re greater than about 50. Indeed when nondimensional quantities are plotted against z/Re there is negligible change above Re about 50 until unsteady or turbulent levels are approached. Han's value for the entrance length is $z/\mathrm{Re} = 0.0752$ and is independent of Re, while Goldstein and Kreid give a value of $z/\mathrm{Re} = 0.090$ for the higher Re; they comment however on the difficulty of finding the intersection of a straight line and their almost parallel experimental curve. These values should be compared with the value of $z/\mathrm{Re} = 0.0099$ for the two-dimensional flow between parallel plates. Thus it can be seen that the error in using a two-dimensional value for the entrance length is significant, the three-dimensional length being about eight times greater. It should also be noted that the fully developed center line axial velocities are 1.50 and 2.096 in the two- and three-dimensional cases, respectively, again pointing to the difficulties of assuming two-dimensional values.

In Fig. 5 the axial component (w) of the velocity on the center line of the duct is

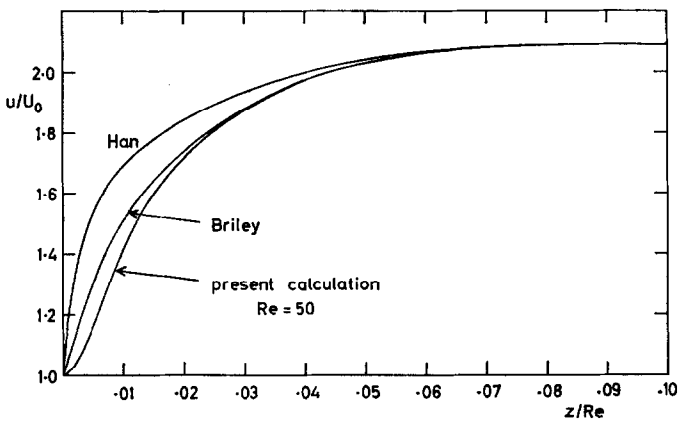

FIG. 5. Axial component of the centerline velocity plotted against z/Re, for flow in a square duct.

plotted against z/Re. Differences close to the entrance are to be expected from the discussion above, but for $z/\mathrm{Re} \geqslant 0.02$ good agreement is obtained. The experimental points are not plotted but lie very close to the present results, see [12]. The results of Han [11] are everywhere a fraction on the high side. The rather slower development of the flow close to the entrance obtained from the present calculations was to be expected since this region is treated more accurately. The results are similar to those

obtained for the corresponding two-dimensional case. The outer walls slow down the uniform inlet flow and to compensate, a rather faster flow develops a little way in from the boundaries. After a short distance down the duct the axial component of the center line velocity catches up and eventually has the maximum velocity. Then the comparison with the boundary layer solution becomes valid.

8. Flow in a Square Duct with a Recess on One Wall

The region of the flow is illustrated in Fig. 6. The problem provides an interesting application of the method to a situation of practical importance. Such configurations occur in many fluid handling devices. At high enough velocities, eddies are shed from the lips of the recess and these can cause excessive noise. The eddy shedding is time dependent and cannot be studied by the present steady calculations but the steady region up to shedding speeds can be treated.

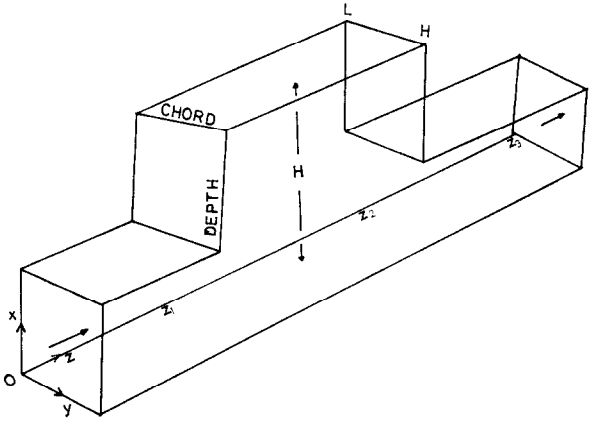

Fig. 6. Schematic drawing of the region of flow for cavity problem.

The boundary conditions on the solid walls are treated similarly to those of the previous section and the inlet and outlet conditions are precisely those of Section 7. The additional difficulty is the reentrant lines. The only component of the vorticity required on these lines is $\xi_2 = \partial u/\partial z - \partial w/\partial x$ and the method of treatment was discussed at the end of Section 3 and illustrated in Fig. 3.

The same geometry was studied experimentally by Lewis [14]. He used a constant Re $\simeq$ 4500 and varied the depth/chord ratio (d/c). This Re is rather high so that detailed *quantitative* comparisons with the present calculations are not given. The results in the present case are for Re = 1, 50, 100 and 500 with $d/c = 0.5, 1, 1.5, 2$. Typically for $d/c = 1$ an $18 \times 10 \times 38$ mesh was used with $\Delta x = \Delta y = \Delta z = 0.125$. For the higher Re the entrance length is well beyond the end of the duct but it was impractical computationally to make the duct any longer. The imposed fully developed

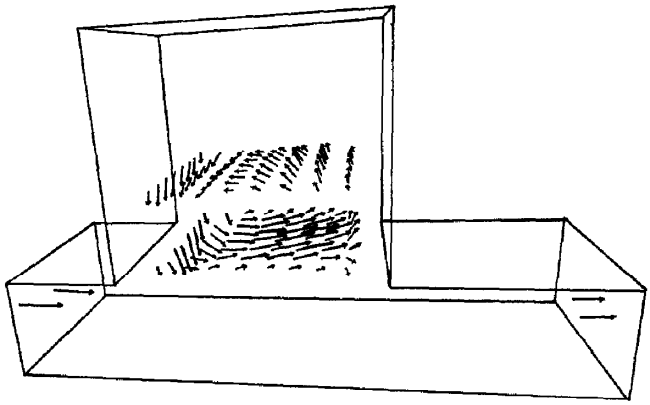

FIG. 7. Velocity vector distribution in the cavity with Re = 50 and depth/chord ratio equal to 1.

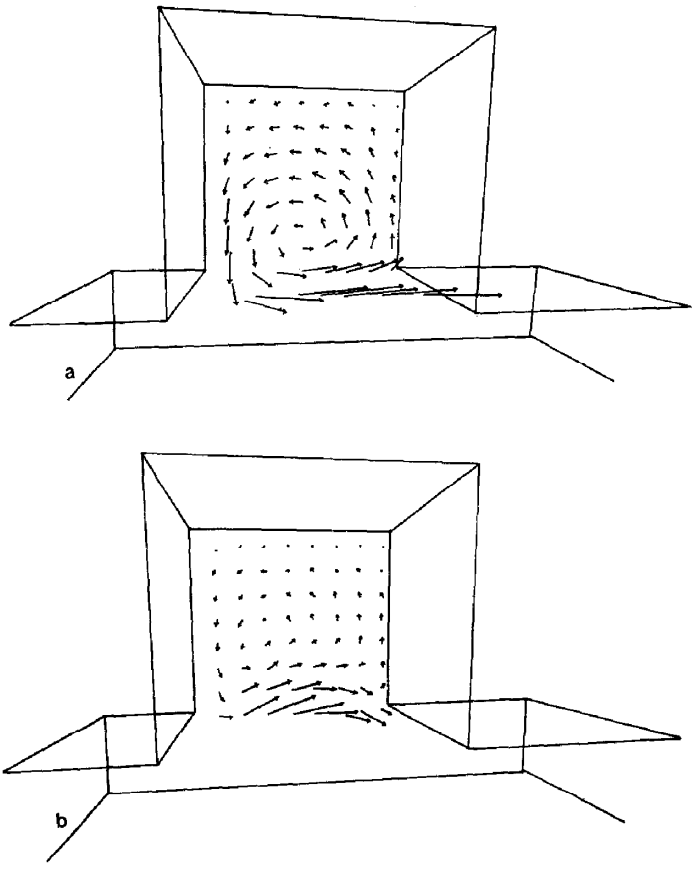

FIG. 8. Velocity vector distribution in plane ($y = 0.5$) in the cavity with depth/chord ratio equal to 1. In 4(a) Re 50 and Re = 1 in 4(b).

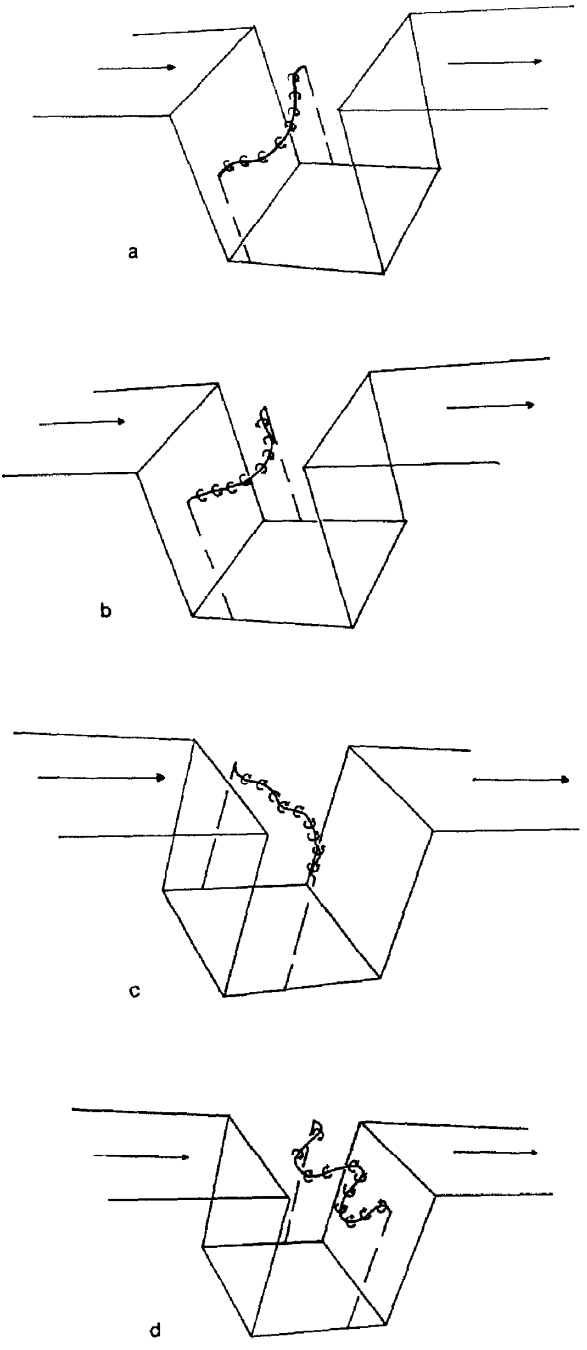

FIG. 9. Vortex flow pattern at depth/chord ratio equal to 1. (a) Re = 1, (b) Re = 50, (c) Re = 100, (d) Re = 500.

flow at the exit must have some effect on the mainstream flow but it would not be expected to affect the flow in the cavity too much.

The flow in the cavity is weak and difficult to illustrate. However, in Fig. 7 vectors proportional to the velocity at a mesh of points in two planes of the cavity are plotted. It shows the complicated three-dimensional nature of the flow. In Fig. 8 slices through the center line of the duct are taken and the velocities are plotted to compare the effect of Re.

A useful concept used by Lewis to simplify the plots is to locate the center of the vortex. On each plane y = constant, the center of the vortex is found and these are then plotted on a perspective diagram. With $d/c = 1$ this vortex center is shown in Fig. 9 for Re = 1, 50, 100, 500. For Re = 1, 50 the vortex center is U-shaped while for Re = 100 it is on the point of changing to a W-shaped vortex which is clearly seen for the case Re = 500. In all cases the vortex center is almost planar with the plane rotating through about a right angle as Re increases. The stagnation point in the cavity moves downstream as Re increases and is shown in Fig. 10. Extremely weak secondary eddies are observed in the corners of the recess but are too small to show up clearly in the figures.

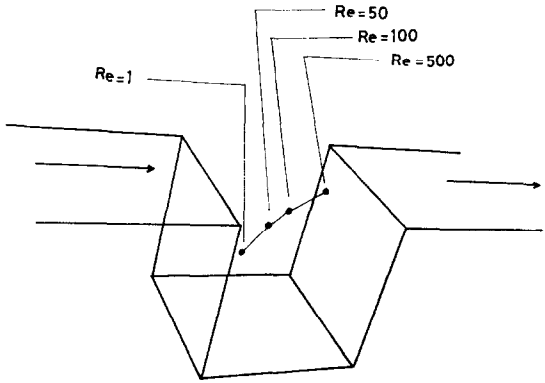

FIG. 10. Distribution of the stagnation points with varying Reynolds number. Depth/chord ratio is 1.

In order to study the effect of changes of geometry the case Re = 50 was chosen and d/c took values 0.5, 1, 1.5, 2.0. The vortex filament for $d/c = 1$ is illustrated in Fig. 9b while the cases $d/c = 0.5$, 2.0 are shown in Fig. 11; the case $d/c = 1.5$ is not given. For $d/c = 0.5$ the situation seems to be on the point of changing to a U-shaped vortex filament, while for larger values the U becomes more pronounced and has a progressively flatter base. The base becomes almost a straight line nearer to the midplane as d/c increases. A very weak secondary vortex may be seen in Fig. 11b in the bottom corner of the cavity; it is just strong enough to be shown. It appears that for the largest values of d/c two-dimensional slices parallel to the flow direction should give reasonable agreement in the cavity.

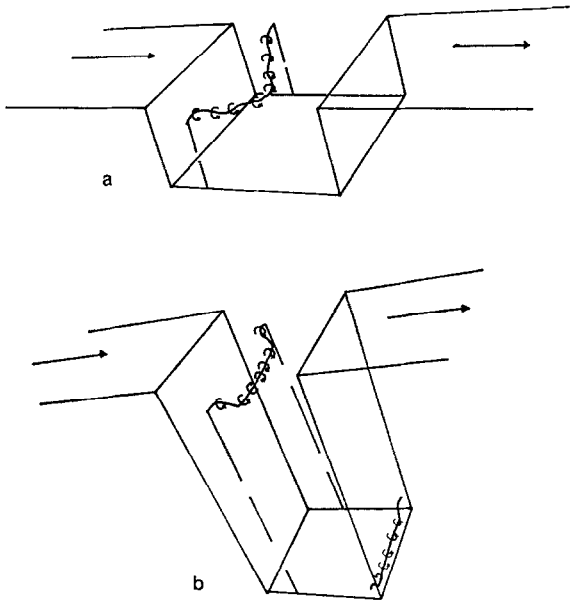

FIG. 11. Vortex flow pattern with Re = 50. (a) Depth/chord ratio = 0.5; (b) depth/chord ratio = 2.

In experiments, Lewis [14] worked with water at the single inlet speed of 15 ft/sec and a 4-inch square entrance. Thus Re $\simeq$ 4500 and is very much higher than those used above. It was not possible to get convergence of the theoretical calculations within reasonable computing times for Re much greater than the value of 500 used.

For d/c between 0.25 and 0.8 a U-vortex was observed by Lewis but the plane of the U could have two orientations both apparently stable. At $d/c = 0.8$ an abrupt change to a W-vortex was observed. The plane of W was more or less in the diagonal plane of the recess from the upstream lip. As d/c increased to about 1.25 the W-vortex persisted with the plane of the vortex rotating through a right angle to the opposite diagonal plane from the downstream lip. Above this value of d/c the flow was reported to be chaotic.

Although detailed comparisons are not possible it should be noted that both the present calculations and Lewis' experiments show similar features. They both show the complicated three-dimensional nature of the flow. In each case U- and W-vortices occur and are almost planar. The planes of the vortices also rotate with changes of either geometry or Re. These similarities give considerable encouragement that work on three-dimensional flows is both necessary and fruitful.

ACKNOWLEDGMENTS

Y.A.S.A. would like to thank the Association of Commonwealth Universities and the University of Ife, Nigeria for support while this work was being undertaken.

REFERENCES

1. K. AZIZ AND J. D. HELLUMS, *Phys. Fluids* **10** (1967), 314.
2. G. D. MALLINSON AND G. DE VAHL DAVIS, *J. Computational Phys.* **12** (1973), 435.
3. P. H. HOLST AND K. AZIZ, *Int. J. Heat Mass Transfer* **15** (1972), 73.
4. G. J. HIRASAKI AND J. D. HELLUMS, *Quart. Appl. Math.* **26** (1968), 331.
5. G. J. HIRASAKI AND J. D. HELLUMS, *Quart. Appl. Math.* **28** (1970), 293.
6. R. COURANT, E. ISAACSON, AND M. REES, *Comm. Pure Appl. Math.* **5** (1952), 243.
7. J. D. HELLUMS AND S. W. CHURCHILL, *Amer. Inst. Chem. Eng. J.* **8** (1962), 690, 693.
8. A. D. GOSMAN, W. M. PUN, A. K. RUNCHAL, D. B. SPALDING, AND M. WOLFSTEIN, "Heat and Mass Transfer in Recirculating Flows," Academic Press, New York/London, 1969.
9. A. J. CHORIN, *Math. Comp.* **22** (1968), 745.
10. D. F. ROSCOE, *Int. J. Numer. Methods Eng.* **10** (1976), 1299.
11. L. S. HAN, *J. Appl. Mech.* **27** (1960), 403.
12. W. R. BRILEY, *J. Computational Phys.* **14** (1974), 8.
13. R. J. GOLDSTEIN AND D. K. KREID, *J. Appl. Mech.* **34** (1967), 813.
14. W. E. LEWIS, Thermodynamics and fluid mechanics convention 1966, *Proc. Inst. Mech. Eng.* **180** (35), Paper 18, 102.